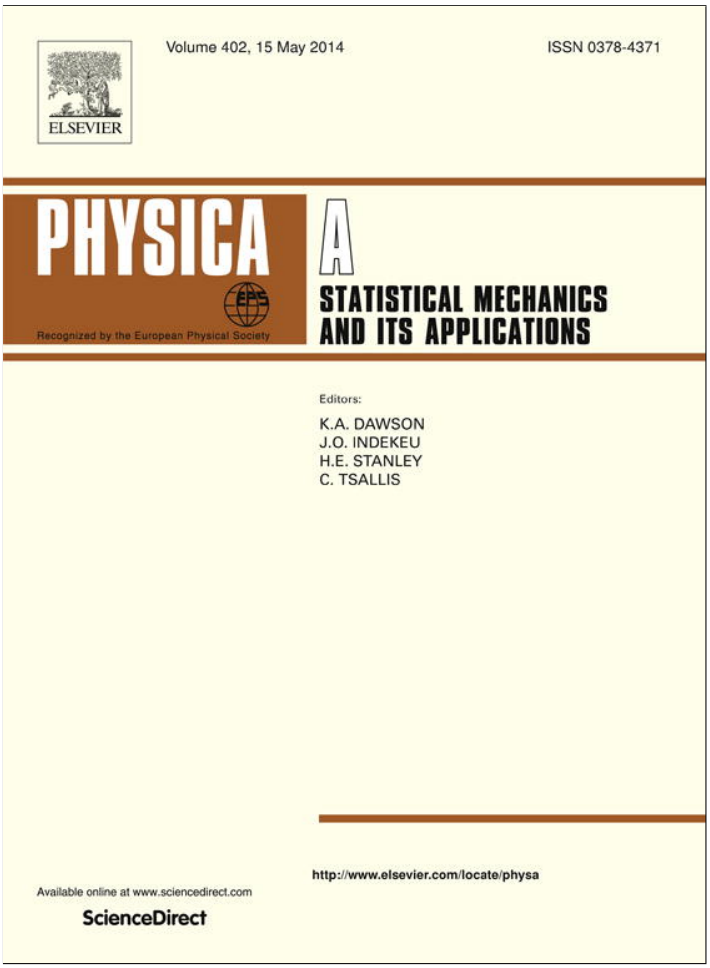

Physica A 402 (2014) 150–168

Contents lists available at ScienceDirect

Physica A

journal homepage: www.elsevier.com/locate/physa

Mixed convection of copper–water nanofluid in a shallow inclined lid driven cavity using the lattice Boltzmann method

Arash Karimipour [a,*], Mohammad Hemmat Esfe [a], Mohammad Reza Safaei [b], Davood Toghraie Semiromi [c], Saeed Jafari [d], S.N. Kazi [b]

[a] Department of Mechanical Engineering, Najafabad Branch, Islamic Azad University, Isfahan, Iran
[b] Department of Mechanical Engineering, University of Malaya, 50603 Kuala Lumpur, Malaysia
[c] Department of Mechanical Engineering, Khomeinishahr Branch, Islamic Azad University, Isfahan, Iran
[d] Department of Petroleum Engineering, School of Engineering, Shahid-Bahonar University of Kerman, Kerman, Iran

HIGHLIGHTS

- Nanofluid LBM simulation in a shallow inclined driven cavity for the first time.
- Showing appropriate ability of LBM to simulate nanofluid mixed convection.
- Sharp increasing in Nu_m with γ and φ especially at higher Ri.
- More Nu_m is observed at $Re = 100$ than the state of $Re = 10$.
- Obtaining higher Nu_m at a vertical position of free convection in higher Re and φ.

ARTICLE INFO

Article history:
Received 5 July 2013
Received in revised form 1 January 2014
Available online 31 January 2014

Keywords:
Shallow inclined cavity
Nanofluid
Lattice Boltzmann
Mixed convection

ABSTRACT

The goal of this work is to study the laminar mixed convection of water–Cu nanofluid in an inclined shallow driven cavity using the lattice Boltzmann method. The upper lid of the cavity moves with constant velocity, U_0, and its temperature is higher than that of the lower wall. The side walls are assumed to be adiabatic. The effects of different values of the cavity inclination angle and nanoparticles volume fraction at three states of free, force and mixed convection domination are investigated while the Reynolds number is kept fixed as $Re = 100$ and $Re = 10$. Validation of present results with those of other available ones shows a suitable agreement. Streamlines, isotherms, Nusselt numbers, and velocity and temperature profiles are presented. More Nusselt numbers can be achieved at larger values of the inclination angle and nanoparticles volume fraction at free convection domination. Results imply the appropriate ability of LBM to simulate the mixed convection of nanofluid in a shallow inclined cavity.

1. Introduction

Lattice Boltzmann method (LBM) is a type of CFD methods which is applied for the numerical simulation of flow and heat transfer. LBM can be used for macro, micro and nano flows (MEMS & NEMS) and its suitable performance has led to an

* Corresponding author. Tel.: +98 9133251252.
E-mail addresses: arashkarimipour@gmail.com, arash.karimipour@yahoo.com (A. Karimipour), M.hemmatesfe@gmail.com (M. Hemmat Esfe), cfd_safaei@yahoo.com (M.R. Safaei), Toghraee@iaukhsh.ac.ir (D. Toghraie Semiromi), saeed.jafari.1362@gmail.com (S. Jafari), Salimnewaz@um.edu.my (S.N. Kazi).

http://dx.doi.org/10.1016/j.physa.2014.01.057
0378-4371/

Nomenclature

BGK Bhatnagar Gross Krook
$\mathbf{c} = (c_x, c_y)$ Microscopic velocity vector
Cu copper
C_p Heat capacity, J kg^{-1} K^{-1}
d_p Nanoparticle diameter, nm
DSMC Direct simulation Monte Carlo
e Internal energy density
f, g Density-momentum and internal energy density distribution functions
$\mathbf{g}$ Gravity vector
$\mathrm{Gr} = g\beta_{nf}H^3\Delta T/\upsilon_{nf}^2$ Grashof number
GPTBC General purpose thermal boundary condition
h, l Cavity height and length, m
$H = h/h, L = l/h$ Dimensionless height and length
k Thermal conductivity coefficient, Wm^{-1} K^{-1}
LBM Lattice Boltzmann method
Ma Mach number
MEMS Microelectromechanic systems
MD Molecular dynamic
Nu_X, Nu_m Local and averaged Nusselt number
NS Navier–Stokes
$\mathrm{Pr} = \upsilon_{nf}/\alpha_{nf}$ Prandtl number
$\mathrm{Re} = \rho_{nf}U_0h/\mu_{nf}$ Reynolds number
$\mathrm{Ri} = \mathrm{Gr}/\mathrm{Re}^2$ Richardson number
t Time, s
T_H, T_C Hot and cold Temperature, K
$\mathbf{u} = (u, v)$ Macroscopic flow velocity vector, ms^{-1}
$(U, V) = (u/U_0, v/U_0)$ Dimensionless flow velocity in x–y direction
U_0 Cavity lid velocity, ms^{-1}
x, y Cartesian coordinates, m
$(X, Y) = (x/h, y/h)$ Dimensionless coordinates
Z Heat dissipation

Greek symbols

α Thermal diffusivity, m^2 s^{-1}
φ Nanoparticles volume fraction
μ Dynamic viscosity, Pa s
$\theta = (T - T_C)/(T_H - T_C)$ Dimensionless temperature
ρ Density, kg m^{-3}
τ_f, τ_g Relaxation times for momentum and internal energy
υ Kinematics viscosity, m^2 s^{-1}
γ Cavity inclination angle
Ω Collision operator

Super- and sub-scripts

e Equilibrium
f Base fluid (pure water)
i Lattice directions
nf Nanofluid
s Solid nanoparticles
w Wall
α x–y geometry components

increase in its usage in different conditions. Basically, LBM is a compressible model of ideal gas; so, it is able to satisfy the compressible Navier–Stokes (NS) equations. However, by using the Chapman–Enskog expansion, the incompressible NS equations would be achieved; and also, at low values of the Mach number, the compressibility error of LBM is negligible [1–8]. LBM is also more appropriate to simulate the multiphase flows compared to the Navier–Stokes equations. LBM uses the

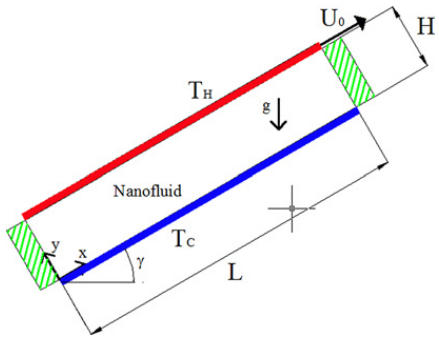

Fig. 1. The schematic of the shallow inclined cavity.

first-order PDEs which makes it a simple approach in discretization and programming. Applying parallel processing and not needing additional system of equations for the pressure field are some other advantages of LBM. Moreover, it is less time-consuming than the other particle based methods such as molecular dynamic, MD, or direct simulation Monte Carlo, DSMC [9–12]. The flow simulation in LBM, is performed by the collision and streaming of the fictive particles located on the lattice nodes; however, it is supposed that the BGK model is applied as the suitable collision operator to satisfy the conservative equations [13–16].

Much attention has been paid to improve LBM usage in micro flows in different conditions [17–25]. Fluid flow and heat transfer in a lid driven cavity is one of the most interesting topics usually considered to solve by LBM. These cavities can be used in many practical engineering and industrial applications such as building thermal-designing optimizations, solar collectors manufacturing, and electronic cooling systems. Moreover, some articles have reported the heat transfer in the shallow cavities due to its possible practical applications. In such cases, the surface effects of the moving wall are getting more important than the volumetric ones [26–29]. Large numbers of papers have proved nice performance of LBM for the natural convection heat transfer [30–32]. In addition, appropriate ability of LBM to simulate the porous media filled in an enclosure, was also shown by Grucelski et al. [33]. Several methods have been presented for the thermal lattice Boltzmann. Among them the internal energy distribution function model, presented by He et al. [34], is nearly the new one which shows the appropriate accuracy and stability, and is able to consider the pressure work and viscous heat dissipation. Karimipour et al. [35] used this model to simulate the air mixed convection in an enclosure.

An innovative way to increase the heat transfer rate is using the mixture of liquid and suspensions of solid nanoparticles called nanofluid [36]. This mixture is supposed to have larger thermal conductivity than the base fluid. A large number of articles can be referred which concern the nanofluid simulation in cavities using Navier–Stokes equations [37–44]; like the mixed convection of Cu–water nanofluid in an enclosure with sinusoidal top lid presented by Karimipour et al. [45] or the investigation of nanofluid mixed convection in a shallow cavity using a two-phase mixture model reported by Goodarzi et al. [46]. They showed the effects of the volume fraction on turbulent kinetic energy, turbulence intensity, skin friction and wall shear stress are insignificant in a shallow cavity. Meanwhile, the nanofluid flow was tried in different conditions; for instance in a tube or through the two isothermally heated parallel plates or even in micro and minichannels etc. [47–51]. The channel with a characteristic length of 3 mm was called minichannel in their work.

In recent years, researchers have tried to simulate the nanofluid natural convection by LBM, and some successes have been achieved [52–56]. However, there are a few articles concerning the nanofluid mixed convection by LBM such as what was done by Nemati et al. [57]. Moreover, in all of them, driven cavity is in horizontal position where the sidewalls are aligned with the direction of gravity. It might be necessary to use the inclined cavity in some applications. In this state, the shear of lid driven may be assisting or opposing the buoyancy forces [58].

So, in the present paper, nanofluid mixed convection in an inclined shallow lid driven cavity is studied by LBM for the first time (to the best of author's knowledge). The shallow condition is selected to present the possible practical applications. Using LBM, the Boltzmann collision term and hydrodynamic boundary conditions should be modified to include both buoyancy forces and inclination angle effects together with the cavity lid motion.

2. Problem statement

Laminar mixed convection of water–Cu nanofluid in an inclined shallow cavity ($AR = L/H = 5$) is studied using lattice Boltzmann method as shown in Fig. 1. Density-momentum distribution function, f, is used for the hydrodynamic properties and internal energy density distribution function, g, is also applied for the thermal properties. The hot upper lid moves with constant velocity, U_0. Side walls are assumed to be adiabatic. Nanofluid is a Newtonian homogeneous dispersion of nanoparticles of copper (Cu) in the pure water (base fluid). The spherical nanoparticles diameter is $d_p = 10$ nm.

The effects of different values of cavity inclination angle ($\gamma = 0, \gamma = 30, \gamma = 60$ and $\gamma = 90°$) and nanoparticles volume fraction ($\varphi = 0.0, \varphi = 0.02$ and $\varphi = 0.04$) in three states of free (Ri = 10), mixed (Ri = 1) and force (Ri = 0.1) convection domination are investigated while Reynolds number is kept fixed as Re = 100. At present work, Reynolds, Prandtl and Nusselt numbers are determined according to nanofluid characteristics as $\mathrm{Re} = \rho_{nf} U_0 h/\mu_{nf}$, $\mathrm{Pr} = \upsilon_{nf}/\alpha_{nf}$ and

$\mathrm{Nu} = h(\partial T/\partial y)/\Delta T$. Nusselt number expresses the heat transfer rate from the cavity walls and Prandtl number indicates the working fluid properties. So that, any variation in Richardson number ($\mathrm{Ri} = \mathrm{Gr}/\mathrm{Re}^2$) just leads to a change in Grashof number, $\mathrm{Gr} = g\beta_{nf}H^3\Delta T/\upsilon_{nf}^2$, and its effects. It can be said that Ri represents the ratio of buoyancy forces (Gr) versus external tensions of sliding lid (Re) [26]. To show the effect of Re on heat transfer rate, nanofluid Nusselt number variation is also studied at $\mathrm{Re} = 100$ and $\mathrm{Re} = 10$ in last section of the present article.

3. Formulation

3.1. Nanofluid

The effective density of nanofluid with volume fraction φ is written as:

$$\rho_{nf} = \varphi\rho_s + (1-\varphi)\rho_f \tag{1}$$

in which the subscripts nf, f and s indicate the nanofluid, fluid and solid nanoparticles, respectively.

Nanofluid heat capacity and thermal diffusivity can be obtained by Ref. [59]:

$$\left(\rho C_p\right)_{nf} = (1-\varphi)\left(\rho C_p\right)_f + \varphi\left(\rho C_p\right)_s \tag{2}$$

$$\alpha_{nf} = k_{nf}/(\rho C_p)_{nf}. \tag{3}$$

The Brinkman [60] and Chon et al. models [61], are used to express the effective dynamic viscosity and thermal conductivity as follows:

$$\mu_{nf} = \mu_f/(1-\varphi)^{2.5} \tag{4}$$

$$\frac{k_{nf}}{k_f} = 1 + 64.7\times\varphi^{0.7460}\left(\frac{d_f}{d_p}\right)^{0.3690}\left(\frac{k_s}{k_f}\right)^{0.7476}\left(\frac{\mu}{\rho_f\alpha_f}\right)^{0.9955}\left(\frac{\rho_f B_c T}{3\pi\mu^2 l_{BF}}\right)^{1.2321} \tag{5}$$

where $B_c = 1.3807\times10^{-23}$ J/K and l_{BF} are the Boltzmann constant and water mean free path, respectively. It should be mentioned that the effects of nanoparticles diameter and their Brownian motion have been considered in Eq. (5). Moreover, in that equation, μ is determined by:

$$\mu = A10^{\frac{B}{T-C}}, \qquad C = 140\ (\mathrm{K}), \qquad B = 247\ (\mathrm{K}), \qquad A = 2.414\times10^{-5}\ (\mathrm{Pa\ s}). \tag{6}$$

3.2. Lattice Boltzmann method

Using LBM-BGK, based on the internal energy distribution function, hydrodynamic and thermal Boltzmann equations are obtained as [62]:

$$\frac{\partial f_i}{\partial t} + c_{i\alpha}\frac{\partial f_i}{\partial x_\alpha} = \Omega(f) = -\frac{1}{\tau_f}(f_i - f_i^e) \tag{7}$$

$$\frac{\partial g_i}{\partial t} + c_{i\alpha}\frac{\partial g_i}{\partial x_\alpha} = \Omega(g_i) - f_i Z_i = 0.5\left|\mathbf{c}-\mathbf{u}\right|^2\Omega(f_i) - f_i Z_i = -\frac{g_i - g_i^e}{\tau_g} - f_i Z_i. \tag{8}$$

The equilibrium distribution functions are shown as f^e and g^e · $\mathbf{c} = (c_x, c_y)$ and $\mathbf{u} = (u, v)$ are the microscopic and macroscopic velocity vectors, and Ω is the collision operator. τ_f and τ_g are the hydrodynamic and thermal relaxation times.

Qian et al. [63] presented the D2Q9 lattice (Fig. 2) which is found suitable to estimate the discretized microscopic velocities as follows:

$$\begin{aligned}
&\mathbf{c}_i = \left(\cos\frac{i-1}{2}\pi, \sin\frac{i-1}{2}\pi\right), \quad i = 1,2,3,4\\
&\mathbf{c}_i = \sqrt{2}\left(\cos\left[\frac{(i-5)}{2}\pi + \frac{\pi}{4}\right], \sin\left[\frac{(i-5)}{2}\pi + \frac{\pi}{4}\right]\right), \quad i = 5,6,7,8\\
&\mathbf{c}_0 = (0,0).
\end{aligned} \tag{9}$$

The heat dissipation, Z, and equilibrium distribution functions are determined by Eqs. (10)–(12), respectively:

$$Z_i = (c_{i\alpha} - u_\alpha)\left[\frac{\delta u_\alpha}{\delta t} + c_{i\alpha}\frac{\partial u_\alpha}{\partial x_\alpha}\right] \tag{10}$$

$$\begin{aligned}
&f_i^e = \omega_i\rho\left[1 + 3(\mathbf{c}_i\cdot\mathbf{u}) + \frac{9(\mathbf{c}_i\cdot\mathbf{u})^2}{2} - \frac{3\mathbf{u}^2}{2}\right], \quad i = 0,1,\ldots,8\\
&\omega_0 = 4/9, \qquad \omega_{1,2,3,4} = 1/9, \qquad \omega_{5,6,7,8} = 1/36
\end{aligned} \tag{11}$$

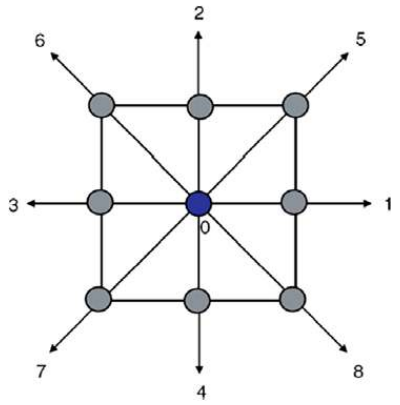

Fig. 2. D2Q9 lattice.

$$g_0^e = -\frac{2}{3}\rho e\mathbf{u}^2$$
$$g_{1,2,3,4}^e = \frac{1}{9}\rho e\left[1.5 + 1.5(\mathbf{c}_{1,2,3,4}\cdot\mathbf{u}) + 4.5(\mathbf{c}_{1,2,3,4}\cdot\mathbf{u})^2 - 1.5\mathbf{u}^2\right] \tag{12}$$
$$g_{5,6,7,8}^e = \frac{1}{36}\rho e\left[3 + 6(\mathbf{c}_{5,6,7,8}\cdot\mathbf{u}) + 4.5(\mathbf{c}_{5,6,7,8}\cdot\mathbf{u})^2 - 1.5\mathbf{u}^2\right].$$

Now discretized forms of hydrodynamic and thermal Boltzmann equations are written as:

$$f_i(\mathbf{x}+\mathbf{c}_i\Delta t, t+\Delta t) - f_i(\mathbf{x},t) = -\frac{\Delta t}{2\tau_f}\left[f_i(\mathbf{x}+\mathbf{c}_i\Delta t, t+\Delta t) - f_i^e(\mathbf{x}+\mathbf{c}_i\Delta t, t+\Delta t)\right] - \frac{\Delta t}{2\tau_f}\left[f_i(\mathbf{x},t) - f_i^e(\mathbf{x},t)\right] \tag{13}$$
$$g_i(\mathbf{x}+\mathbf{c}_i\Delta t, t+\Delta t) - g_i(\mathbf{x},t) = -\frac{\Delta t}{2\tau_g}\left[g_i(\mathbf{x}+\mathbf{c}_i\Delta t, t+\Delta t) - g_i^e(\mathbf{x}+\mathbf{c}_i\Delta t, t+\Delta t)\right]$$
$$-\frac{\Delta t}{2}f_i(\mathbf{x}+\mathbf{c}_i\Delta t, t+\Delta t)Z_i(\mathbf{x}+\mathbf{c}_i\Delta t, t+\Delta t) - \frac{\Delta t}{2\tau_g}\left[g_i(\mathbf{x},t) - g_i^e(\mathbf{x},t)\right] - \frac{\Delta t}{2}f_i(\mathbf{x},t)Z_i(\mathbf{x},t). \tag{14}$$

By solving the implicit forms difficulty of Eqs. (13) and (14), new distribution functions $\tilde{f}_i$ and $\tilde{g}_i$ are presented as:

$$\tilde{f}_i = f_i + \frac{\Delta t}{2\tau_f}(f_i - f_i^e) \tag{15}$$
$$\tilde{g}_i = g_i + \frac{\Delta t}{2\tau_g}(g_i - g_i^e) + \frac{\Delta t}{2}f_iZ_i. \tag{16}$$

Using Eqs. (17) and (18) the collision and propagation steps are performed:

$$\tilde{f}_i(\mathbf{x}+\mathbf{c}_i\Delta t, t+\Delta t) - \tilde{f}_i(\mathbf{x},t) = -\frac{\Delta t}{\tau_f + 0.5\Delta t}\left[\tilde{f}_i(\mathbf{x},t) - f_i^e(\mathbf{x},t)\right] \tag{17}$$
$$\tilde{g}_i(\mathbf{x}+\mathbf{c}_i\Delta t, t+\Delta t) - \tilde{g}_i(\mathbf{x},t) = -\frac{\Delta t}{\tau_g + 0.5\Delta t}\left[\tilde{g}_i(\mathbf{x},t) - g_i^e(\mathbf{x},t)\right] - \frac{\tau_g\Delta t}{\tau_g + 0.5\Delta t}f_iZ_i. \tag{18}$$

Kinematics viscosity, υ, and thermal diffusivity, α, are calculated by using relaxation times:

$$\upsilon = \tau_f RT, \qquad \alpha = 2\tau_g RT. \tag{19}$$

To say more details, Kinematic viscosity is estimated as $\upsilon = \mathrm{Re}/U_0h$. Considering the amount of RT (constant of gas and temperature) and Eq. (19), the value of $\tau_f = \upsilon/RT$ is determined. Now, thermal diffusivity is calculated as $\alpha = \upsilon/\mathrm{Pr}$ and finally the amount of τ_g is found from $\tau_g = \alpha/2RT$.

3.3. Gravity effects

By using Boussinesq approximation [30,34], buoyancy force per unit mass is written as $\mathbf{G} = \beta\mathbf{g}(T - \bar{T})$. Moreover, $F = \mathbf{G}\cdot(\mathbf{c}-\mathbf{u})f^e/RT$ refers to the buoyancy force effects in Boltzmann equation:

$$\frac{\partial f_i}{\partial t} + c_{i\alpha}\frac{\partial f_i}{\partial x_\alpha} = -\frac{1}{\tau_f}(f_i - f_i^e) + F = -\frac{1}{\tau_f}(f_i - f_i^e) + \frac{\mathbf{G}\cdot(\mathbf{c_i}-\mathbf{u})}{RT}f_i^e \tag{20}$$

in which $\mathbf{G} = (|G| \sin\gamma, |G| \cos\gamma)$. Having the same procedure as Section 3.2 and also using $\mathbf{u} = (u, v)$ and $\mathbf{c}_i = (c_{ix}, c_{iy})$, the following equations are written:

$$\begin{aligned}\tilde{f}_i(\mathbf{x} + \mathbf{c}_i\Delta t, t + \Delta t) - \tilde{f}_i(\mathbf{x}, t) &= -\frac{\Delta t}{\tau_f + 0.5\Delta t}\left[\tilde{f}_i - f_i^e\right] + \left(\frac{\Delta t\tau_f}{\tau_f + 0.5\Delta t}\frac{3G(c_{ix} - u)}{c^2}f_i^e\right)\sin\gamma \\ &\quad + \left(\frac{\Delta t\tau_f}{\tau_f + 0.5\Delta t}\frac{3G(c_{iy} - v)}{c^2}f_i^e\right)\cos\gamma \end{aligned} \tag{21}$$

$$\tilde{f}_i = f_i + \frac{\Delta t}{2\tau_f}(f_i - f_i^e) - \frac{\Delta t}{2}F \Rightarrow f_i = \frac{\tau_f\tilde{f}_i + 0.5\Delta t f_i^e}{\tau_f + 0.5\Delta t} + \frac{0.5\Delta t\tau_f}{\tau_f + 0.5\Delta t}F \tag{22}$$

$$\begin{aligned} f_i &= \frac{\tau_f\tilde{f}_i + 0.5\Delta t f_i^e}{\tau_f + 0.5\Delta t} + \frac{0.5\Delta t\tau_f}{\tau_f + 0.5\Delta t}\frac{\mathbf{G}.(\mathbf{c_i} - \mathbf{u})}{RT}f_i^e \\ &= \frac{\tau_f\tilde{f}_i + 0.5\Delta t f_i^e}{\tau_f + 0.5\Delta t} + \left(\frac{0.5\Delta t\tau_f}{\tau_f + 0.5\Delta t}\frac{G(c_{ix} - u)}{RT}f_i^e\right)\sin\gamma + \left(\frac{0.5\Delta t\tau_f}{\tau_f + 0.5\Delta t}\frac{G(c_{iy} - v)}{RT}f_i^e\right)\cos\gamma. \end{aligned} \tag{23}$$

To include the effects of both gravity and cavity inclination angle, macroscopic variables can be determined as:

$$\begin{aligned} \rho &= \sum_i \tilde{f}_i \\ u &= (1/\rho)\sum_i \tilde{f}_i c_{ix} + \frac{\Delta t}{2}G\sin\gamma \\ v &= (1/\rho)\sum_i \tilde{f}_i c_{iy} + \frac{\Delta t}{2}G\cos\gamma \\ \rho e &= \rho RT = \sum_i \tilde{g}_i - \frac{\Delta t}{2}\sum_i f_i Z_i. \end{aligned} \tag{24}$$

3.4. Hydrodynamic boundary conditions

The no-slip boundary condition on the walls is simulated using non-equilibrium bounce back model [64]. This model gives no-mass flow rates on the walls, and reflects the particles in suitable directions to access the equilibrium conditions.

For example, for the west wall, the unknown distribution functions are cleared as:

$$\begin{aligned} \tilde{f}_1 &= \tilde{f}_3 + \frac{2}{3}\rho_w U_w \\ \tilde{f}_8 &= \tilde{f}_6 - \frac{\tilde{f}_4 - \tilde{f}_2}{2} + \frac{1}{6}\rho_w U_w - \frac{1}{2}\rho_w V_w + \frac{\Delta t}{4}\rho_w G(\cos\gamma - \sin\gamma) \\ \tilde{f}_5 &= \tilde{f}_7 + \frac{\tilde{f}_4 - \tilde{f}_2}{2} + \frac{1}{6}\rho_w U_w + \frac{1}{2}\rho_w V_w - \frac{\Delta t}{4}\rho_w G(\cos\gamma + \sin\gamma) \end{aligned} \tag{25}$$

in which subscript w refers to the wall nodes. For other walls and corners, corresponding equations can be obtained similarly.

3.5. Thermal boundary conditions

The general purpose thermal boundary condition (GPTBC) is applied to consider the specified temperature on the hot top wall (T_H) and cold bottom wall (T_C).

For example, for the top wall we have:

$$\begin{aligned} \tilde{g}_7 &= \left(3\rho e + 1.5\Delta t\sum_i f_i Z_i - 3(\tilde{g}_0 + \tilde{g}_1 + \tilde{g}_2 + \tilde{g}_3 + \tilde{g}_5 + \tilde{g}_6)\right)[3.0 - 6U_0 + 3.0U_0^2]\frac{1}{36} \\ \tilde{g}_4 &= \left(3\rho e + 1.5\Delta t\sum_i f_i Z_i - 3(\tilde{g}_0 + \tilde{g}_1 + \tilde{g}_2 + \tilde{g}_3 + \tilde{g}_5 + \tilde{g}_6)\right)[1.5 - 1.5U_0^2]\frac{1}{9} \\ \tilde{g}_8 &= \left(3\rho e + 1.5\Delta t\sum_i f_i Z_i - 3(\tilde{g}_0 + \tilde{g}_1 + \tilde{g}_2 + \tilde{g}_3 + \tilde{g}_5 + \tilde{g}_6)\right)[3.0 - 6U_0 + 3.0U_0^2]\frac{1}{36}. \end{aligned} \tag{26}$$

Table 1
Lattice grid study for Ri = 0.1, Re = 100, Pr = 6.2 and $\gamma = \varphi = 0$ at the point of $X = 2.5$ and $Y = 0.5$.

	Lattice grid		
	500 × 100	750 × 150	1000×200
U	−0.236	−0.233	−0.231
V	0.005	0.006	0.006
θ	0.886	0.891	0.893
Nu_m	4.043	4.051	4.054

A similar procedure is taken for the cold bottom wall. GPTBC model is also used for the adiabatic sidewalls. As an example for the west wall:

$$\begin{aligned}
\tilde{g}_5 &= \frac{1}{12}\left[1.5\Delta t\sum_{i=1}^{8} c_{ix} f_i Z_i + 3(\tilde{g}_3 + \tilde{g}_6 + \tilde{g}_7)\right]\\
\tilde{g}_1 &= \frac{1}{6}\left[1.5\Delta t\sum_{i=1}^{8} c_{ix} f_i Z_i + 3(\tilde{g}_3 + \tilde{g}_6 + \tilde{g}_7)\right]\\
\tilde{g}_8 &= \frac{1}{12}\left[1.5\Delta t\sum_{i=1}^{8} c_{ix} f_i Z_i + 3(\tilde{g}_3 + \tilde{g}_6 + \tilde{g}_7)\right].
\end{aligned} \tag{27}$$

The nanofluid Nusselt numbers along the top and bottom walls are calculated as:

$$\begin{aligned}
\mathrm{Nu}_X &= -\frac{k_{nf}}{k_f}\left(\frac{\partial\theta}{\partial Y}\right)_{Y=0,Y=1}\\
\mathrm{Nu}_m &= \frac{1}{AR}\int_0^{AR} \mathrm{Nu}_X\, \mathrm{d}X.
\end{aligned} \tag{28}$$

As it is well seen, present article's numerical procedure concerns a two-dimensional model (2D) for cavity. It should be mentioned that LBM is encountered some limitations at each different using models as like a 2D-model. Here several points of 2D-LBM are presented which should take them in to account.

LBM is applied in near-incompressible regimes. It means Mach number should be $\mathrm{Ma} = U^*/c_s \ll 1$ during the solution process. U^* and c_s are the characteristic velocity and speed of sound, respectively. Characteristic velocity can be written as $U^* = (g\beta\Delta Th)^{0.5}$ and $U^* = \upsilon\mathrm{Re}/H$ for natural convection domination and force convection domination, respectively. In a 2D-LBM simulation $c_s = (1/3)^{0.5}$, so the amount of U^* should be small compared to c_s in all calculations. Moreover, using D2Q9 lattice (2-Dim with 9 points) adds more limitations to present work. For example Eq. (9) just can be used to estimate the microscopic velocities for this kind of lattice; or the equilibrium distribution functions are determined by using Eqs. (11) and (12) only for D2Q9 model. In addition, using a two-dimensional system would have affected the equations of macroscopic variables. For example internal energy is introduced as $e = DRT/2$ in Eq. (24) which D shows the number of geometry dimensions; hence it is equal to 2 at present 2D-work [31,34,35,63].

4. Grid independency and validation

Nanofluid mixed convection is studied using a FORTRAN LBM code. Obtaining lattice nodes independency, the horizontal cavity at Ri = 0.1, Re = 100, and Pr = 6.2 is considered, and the values of U, V, θ and Nu_m at the centre point are reported for pure water in Table 1; due to small differences, the 750 × 150 lattice node is selected for the next computations.

Fig. 3 shows the comparison of U and T along the cavity vertical centreline at $\mathrm{Gr} = 10^2$ and Re = 400 with the results obtained by Iwatsu et al. [29] for the LBM mixed convection. They considered a square enclosure with hot moving top lid and adiabatic sidewalls. More validation is done for water–Cu nanofluid mixed convection with those of Tiwari and Das [38]. They studied a cavity with moving cold and hot side walls. Their results such as Nu_m on the vertical wall and $U_{\max}$ on the vertical centreline at $\mathrm{Gr} = 10^4$ for Ri = 0.1, Ri = 10 and $\varphi = 0.0, \varphi = 0.008$ are shown in Table 2 versus the results obtained in the present article. Appropriate agreements are observed in both Fig. 3 and Table 2 between the present work results and those obtained in previous papers.

5. Results and discussions

Mixed convection of Cu–water nanofluid in a shallow inclined driven cavity (Fig. 1) is studied using LBM. Table 3 illustrates the thermophysical properties of water as the base fluid and the copper as the nanoparticles. $\mathrm{Re} = \rho_{nf} U_0 H/\mu_{nf}$ and $\mathrm{Pr} = \upsilon_{nf}/\alpha_{nf}$ are defined for nanofluid at $\varphi = 0.0\%$ (pure water), $\varphi = 0.02 = 2\%$ and $\varphi = 0.04 = 4\%$.

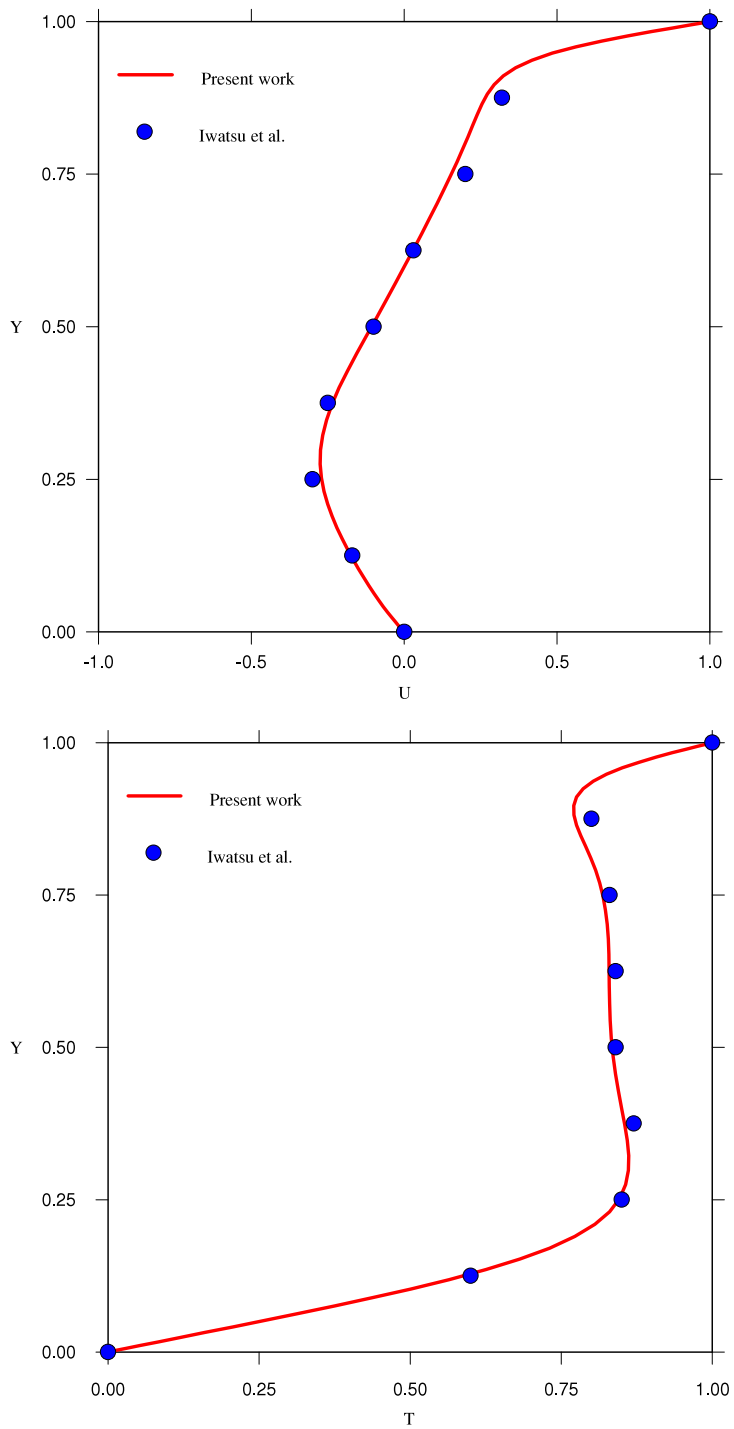

Fig. 3. Comparison of U and T along the cavity vertical centreline for $\mathrm{Gr} = 10^2$ and $\mathrm{Re} = 400$ with those of Iwatsu et al. [29] (square cavity, heated from the top moving wall and cooled from the bottom, with adiabatic sidewalls).

Table 2
Nu_m on the vertical wall and $U_{\max}$ on the vertical centreline obtained from the present work with those of Tiwari and Das [38] at $\mathrm{Gr} = 10^4$ for different Ri and φ.

		$\varphi = 0.0$		$\varphi = 0.08$	
		Present work	Tiwari and Das [38]	Present work	Tiwari and Das [38]
$\mathrm{Ri} = 0.1$	$U_{\max}$	0.51	0.48	0.49	0.46
	Nu_m	32.02	31.64	43.97	43.37
$\mathrm{Ri} = 10$	$U_{\max}$	0.21	0.19	0.20	0.18
	Nu_m	1.41	1.38	1.91	1.85

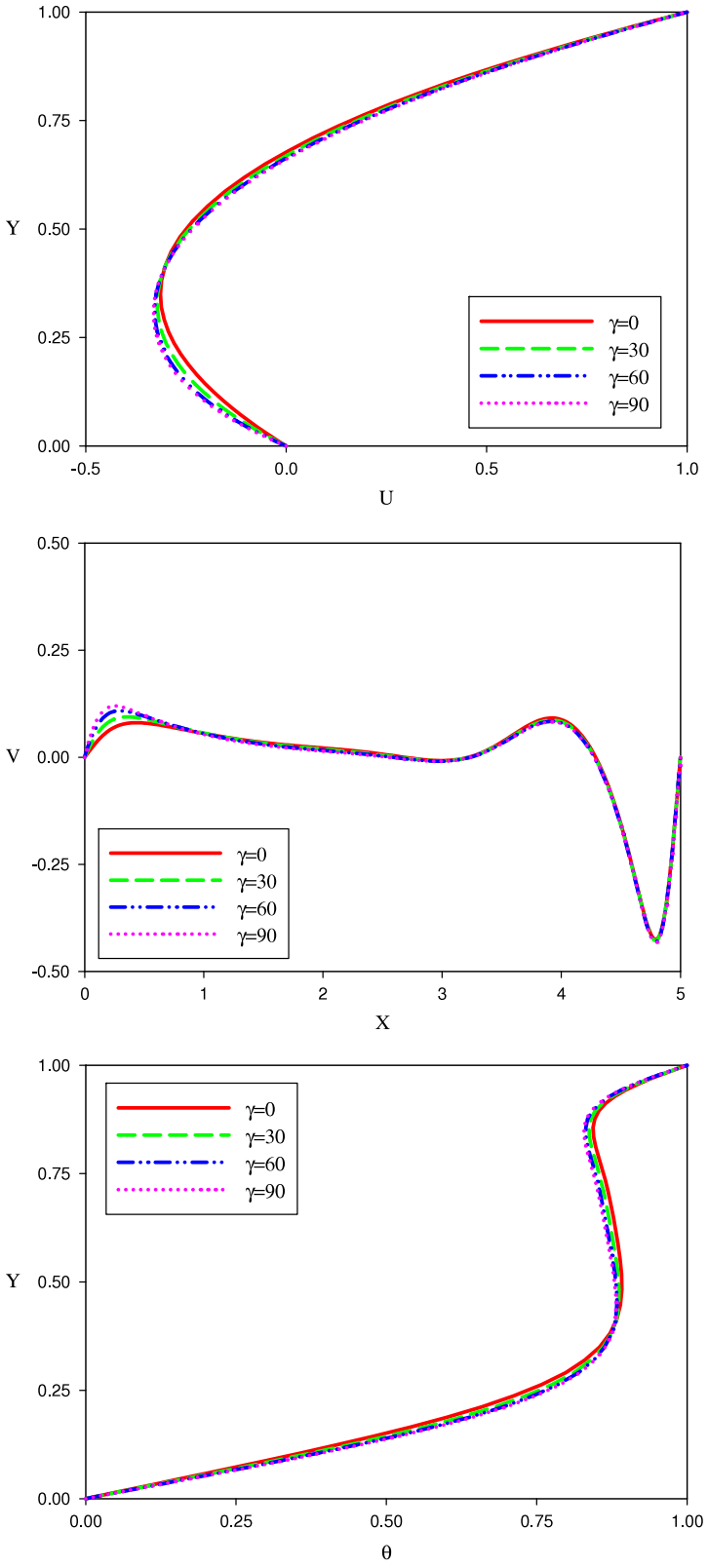

Fig. 4. The profiles of U, θ at $X = 2.5$ and V at $Y = 0.5$ for Ri $= 0.1$ and $\varphi = 0.0$.

5.1. *Effects of the cavity inclination angle*

Fig. 4 shows the dimensionless horizontal velocity profile U, dimensionless temperature profile θ along the cavity vertical centreline and dimensionless vertical velocity profile V along the cavity horizontal centreline for Ri $= 0.1$ of the pure water at different cavity inclination angles, γ. This figure shows $U = 0$ at $Y = 0$, and it approaches the lid velocity at $Y = 1$.

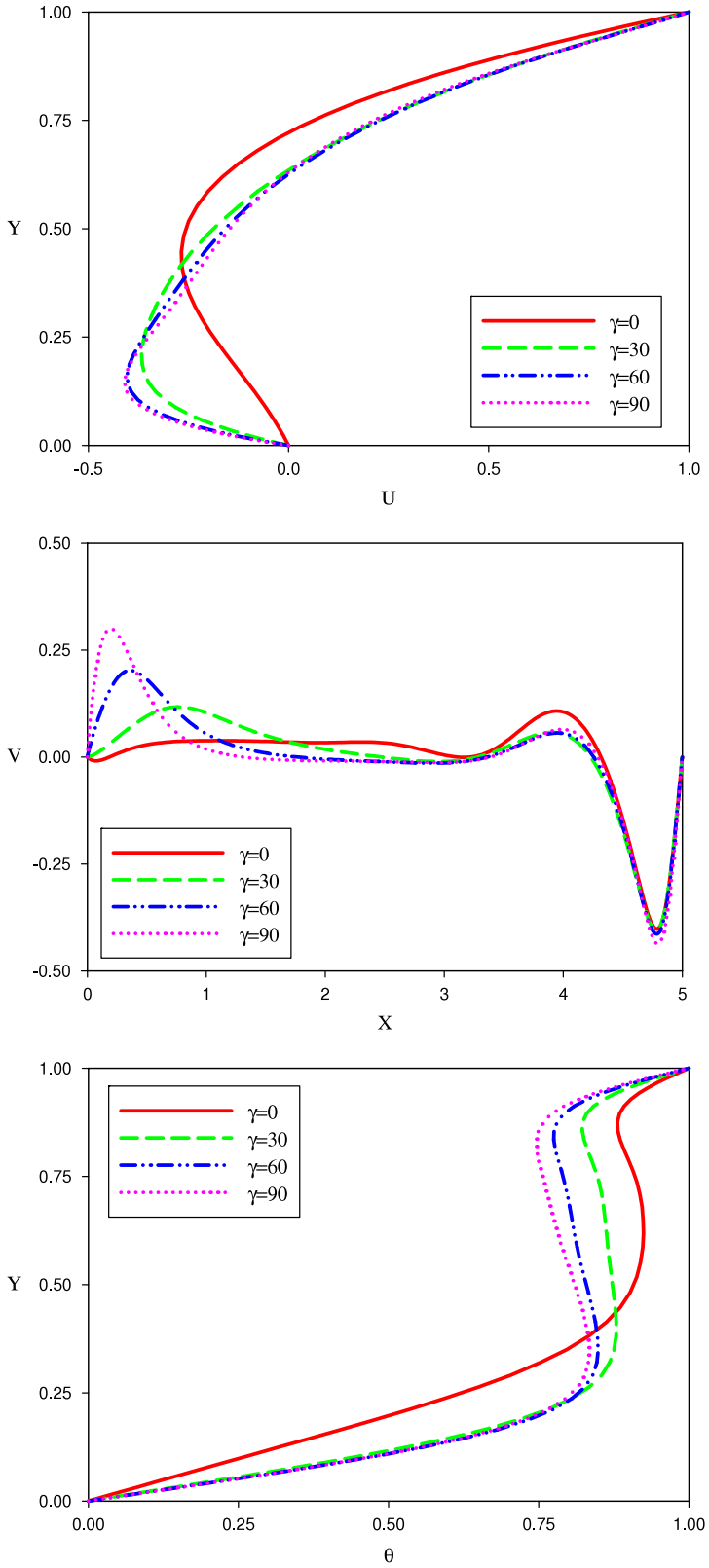

Fig. 5. The profiles of U, θ at $X = 2.5$ and V at $Y = 0.5$ for Ri $= 1$ and $\varphi = 0.0$.

The negative values of U at $0 < Y < 0.75$ show the flow in opposite direction with cavity lid in these areas. Moreover, the powerful downward flow can be seen in V at $4.5 < X < 5$ due to rotational flow in cavity. The temperature profiles, θ, are almost linear at both $0 < Y < 0.25$ and $0.8 < Y < 1$ which indicate more heat transfer than other places. In addition, the constant values of θ at $0.25 < Y < 0.75$ are due to isothermal mass located in the core of supposed rotational flow. It is seen that γ does not have significant effects on U, V and θ in Fig. 4.

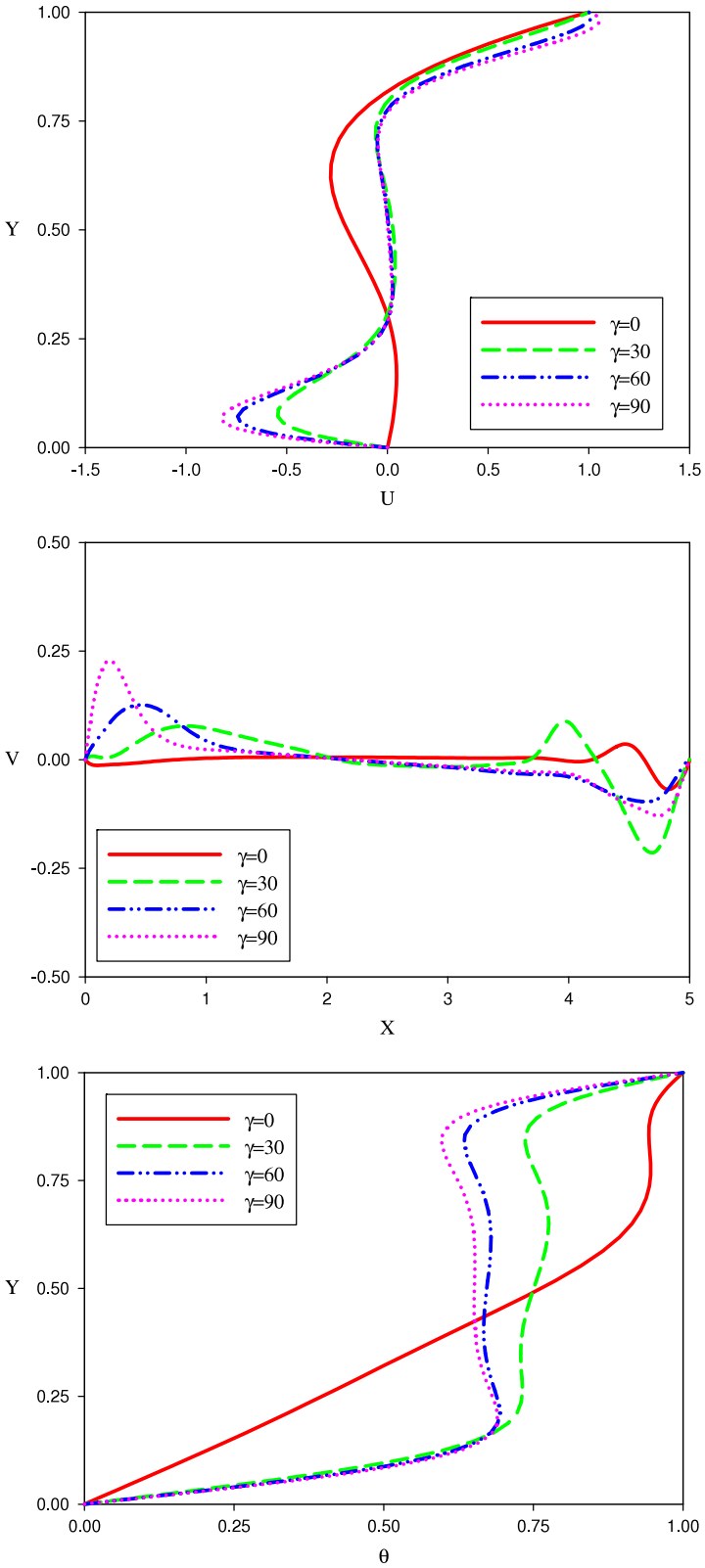

Fig. 6. The profiles of U, θ at $X = 2.5$ and V at $Y = 0.5$ for Ri $= 10$ and $\varphi = 0.0$.

Figs. 5 and 6 show the profiles of U, θ and V for Ri $= 1$ and Ri $= 10$ of the pure water at different γ's. These figures imply how important γ is at more Ri, and that more sensitivity to γ is observed. Constant values of U and θ at $0.25 < Y < 0.75$ and V at $1 < X < 3.5$ for $\gamma = 30$, $\gamma = 60$ and $\gamma = 90^{\circ}$ in Fig. 6, also illustrate the existence of stagnant fluid mass in the core of the rotational cell at these areas. However, at $\gamma = 0$, the variation of θ is almost linear at half down space of cavity. It means nanofluid properties highly depend on γ at more Ri. In this state, results of inclined cavity ($30 \leq \gamma \leq 90$), are

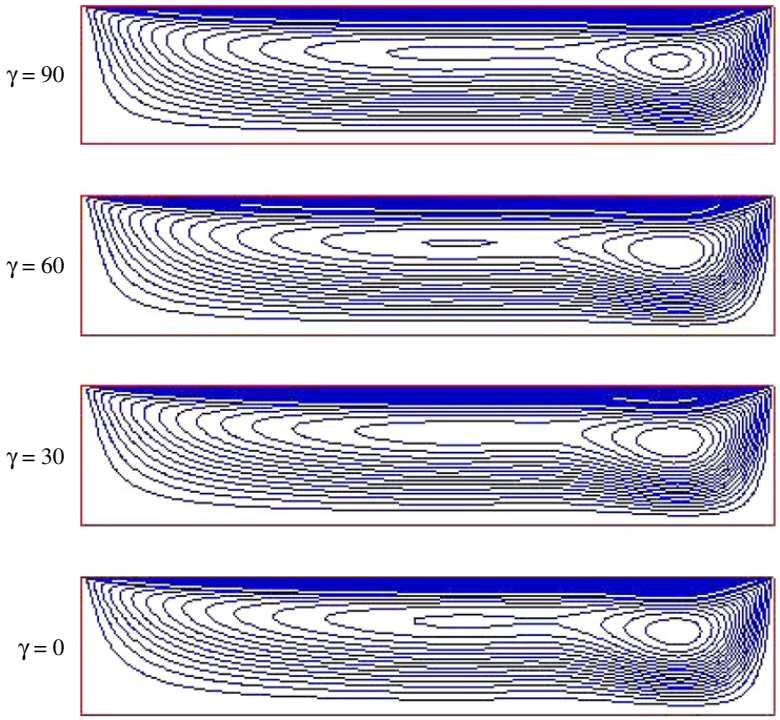

Fig. 7. Streamlines for Ri $= 0.1$ and $\varphi = 0.04$ at different γ.

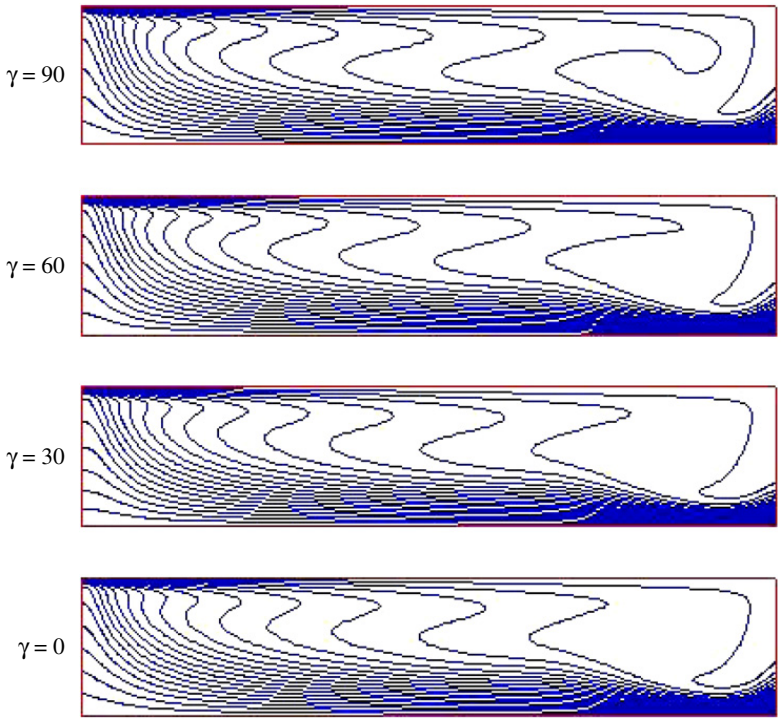

Fig. 8. Isotherms for Ri $= 0.1$ and $\varphi = 0.04$ at different γ.

Table 3
Thermophysical properties of water, copper (Cu) and nanofluid.

	Water	Cu	Nanofluid $\varphi = 0.02$	Nanofluid $\varphi = 0.04$
c_p (J/kg K)	4179	383	3591	3145
ρ (kg/m^3)	997	8954	1156	1315
k (W/mK)	0.6	400	0.9	1.13
μ (Pa s)	8.91×10^{-4}	–	9.37×10^{-4}	9.87×10^{-4}

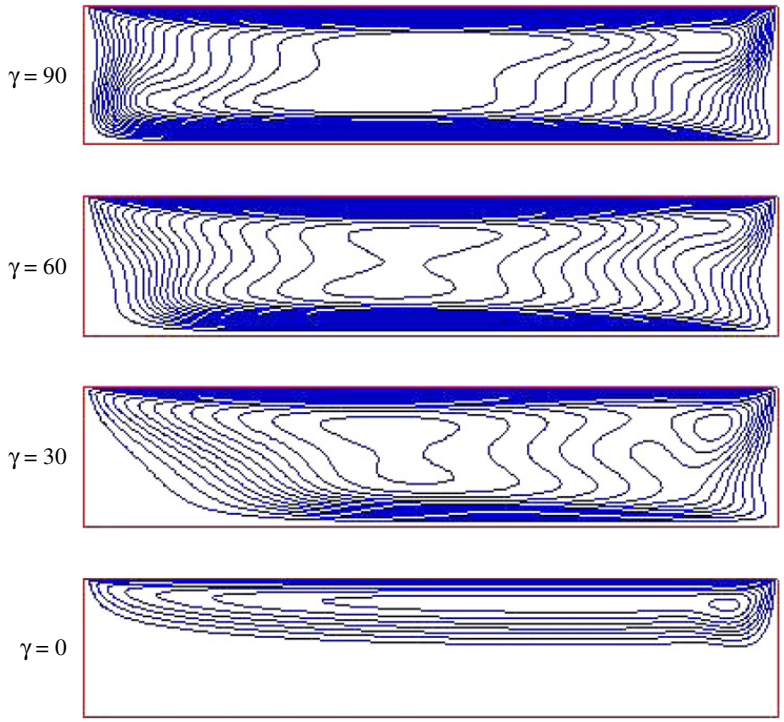

Fig. 9. Streamlines for Ri $=$ 10 and $\varphi = 0.04$ at different γ.

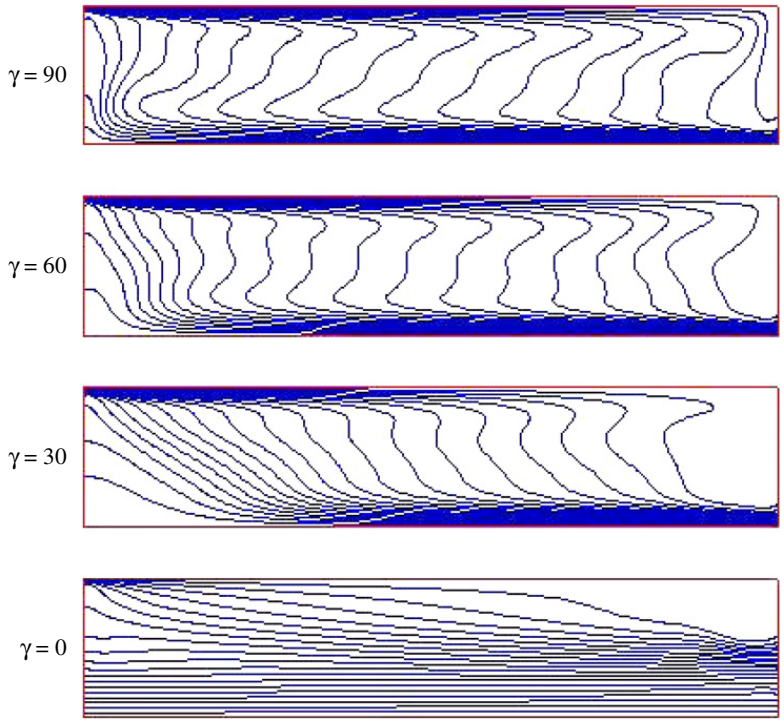

Fig. 10. Isotherms for Ri $=$ 10 and $\varphi = 0.04$ at different γ.

more similar to each other than to the horizontal mode ($\gamma = 0$). Due to the fixed value of Reynolds number as Re $=$ 100, variation of γ leads to change in buoyancy motions.

The effects of surface tensions are usually more important than the volumetric forces in the shallow cavities. It means the flow characteristics should more depend on lid motion at present article. However it is observed that more γ corresponds to support free convection heat transfer. This implies how important free convection could be even in a shallow high aspect ratio cavity especially at inclined and vertical positions.

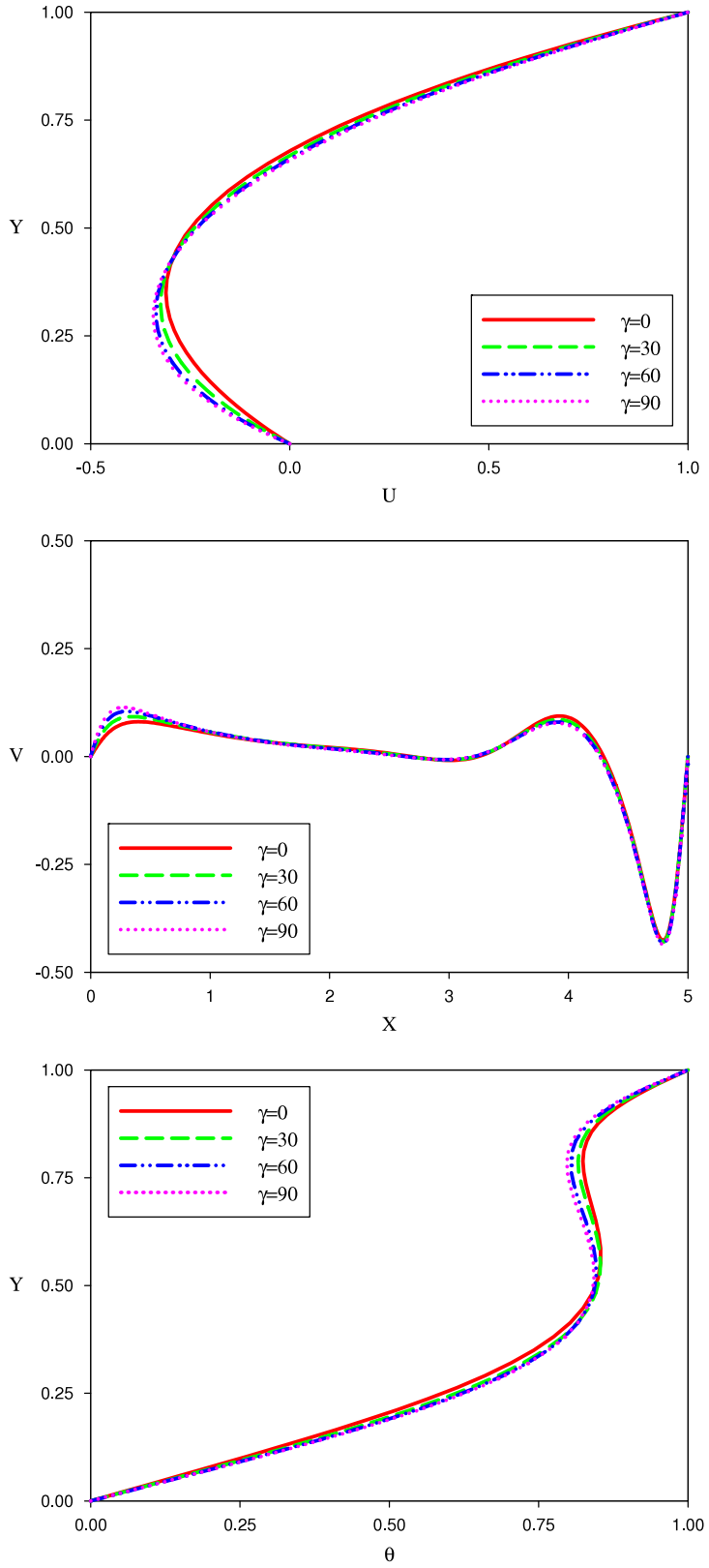

Fig. 11. The profiles of U, θ at $X = 2.5$ and V at $Y = 0.5$ for Ri $= 0.1$ and $\varphi = 0.04$.

5.2. *Effects of nanofluid Richardson number*

Three states of convection domination are investigated. Regarding Richardson number definition, Ri $=$ Gr/Re^2, it is obviously found out that Ri $<$ 1 leads to force convection domination and at Ri $>$ 1, free convection dominates the cavity space. Mixed convection heat transfer would occur at Ri $\approx$ 1.

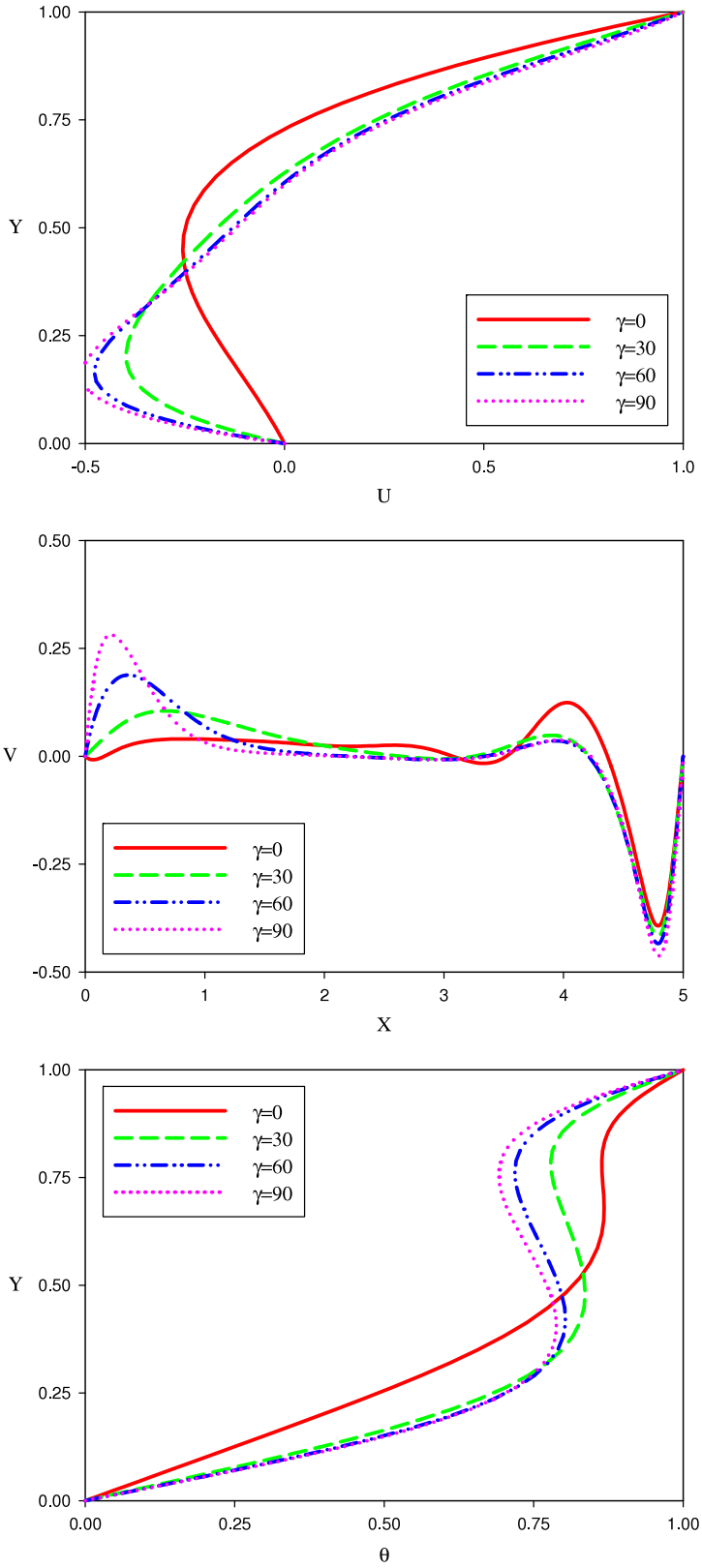

Fig. 12. The profiles of U, θ at $X = 2.5$ and V at $Y = 0.5$ for Ri $= 1$ and $\varphi = 0.04$.

Nanofluid streamlines and isotherms are shown in Figs. 7 and 8 for Ri $= 0.1$ (force convection) and $\varphi = 0.04$ at different γ's. A powerful clockwise cell covers all cavity space (Fig. 7) which has no significant change with γ. The small value of cavity height in comparison to its length corresponds to more sensitivity to the upper wall motion especially at force convection domination (Ri $= 0.1$). The effects of lid motion on its adjacent fluid layers lead to generate a cell which carries the hot fluid to lower spaces; after that, buoyancy effects drive the hot fluid to the upper parts, and so on. Consequently, there will be a

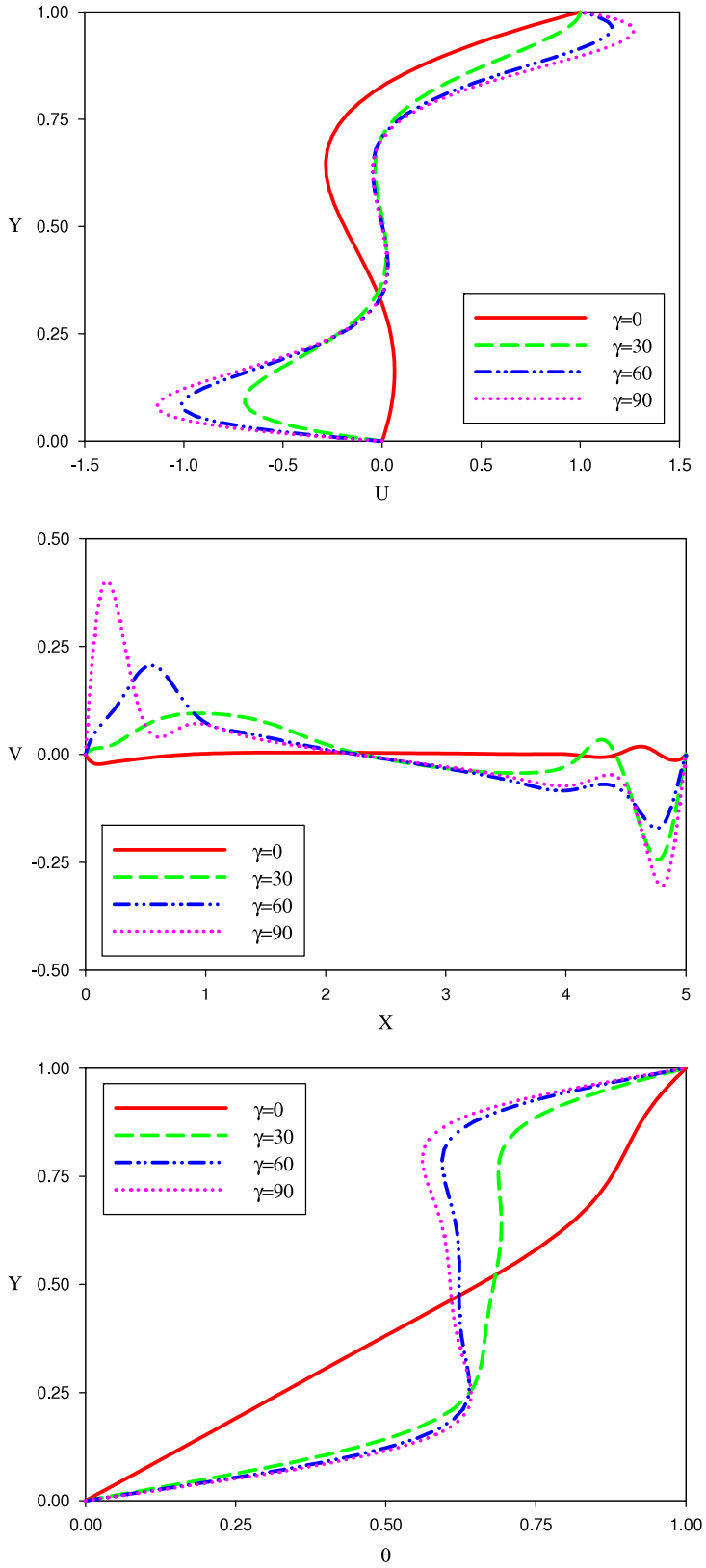

Fig. 13. The profiles of U, θ at $X = 2.5$ and V at $Y = 0.5$ for Ri $= 10$ and $\varphi = 0.04$.

combination of lid motion and buoyancy forces effects called mixed convection. Any change of Ri corresponds to a change in Gr because Reynolds number is kept fixed. So, at Ri $= 0.1$, the movement of cavity lid has more effects on nanofluid than the buoyancy motions.

Nanofluid streamlines for Ri $= 10$ (free convection domination) and $\varphi = 0.04$ at different γ's are presented in Fig. 9. A long cell covers upper half of cavity at $\gamma = 0$ which shows the weak effect of moving lid on lower cavity space. However

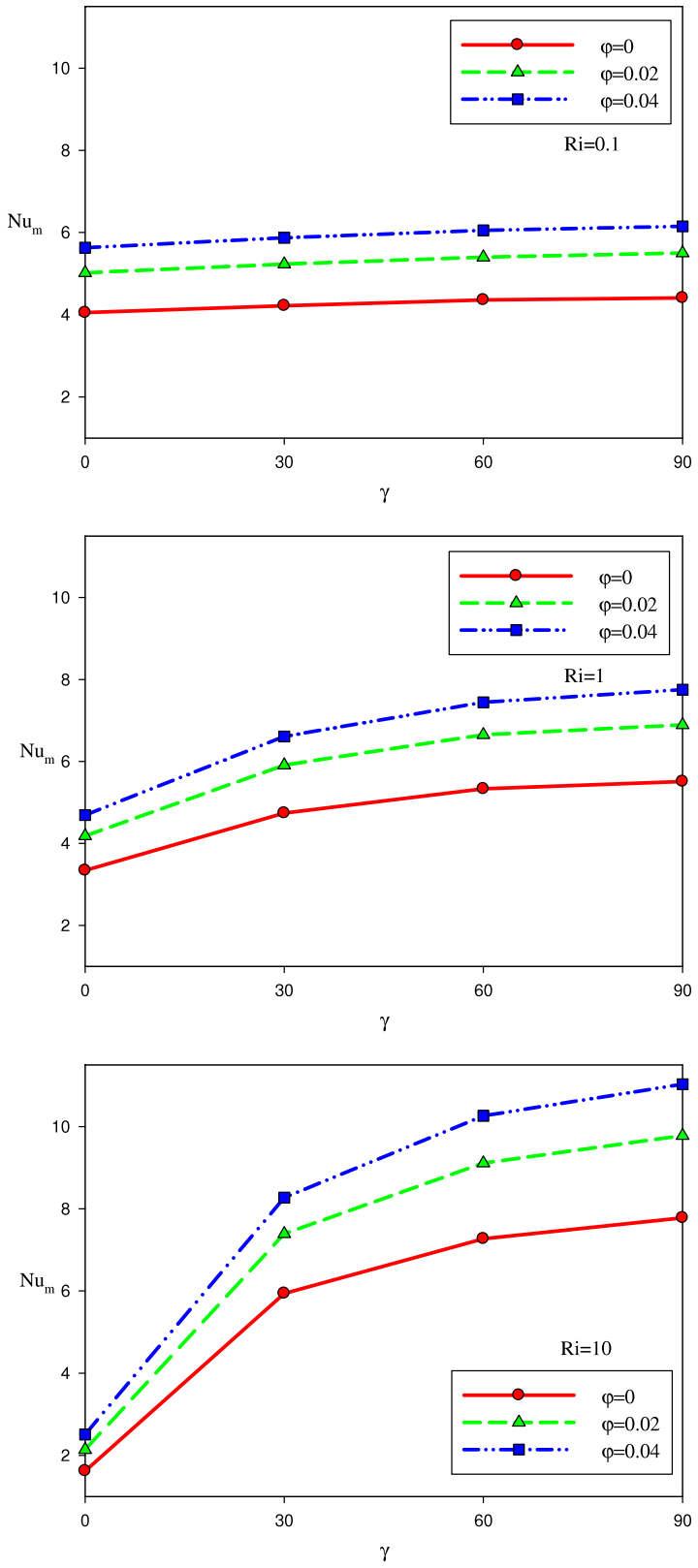

Fig. 14. Nu_m with different values of φ and Ri at Re $=$ 100.

this cell operation domain will penetrate to almost all cavity space at higher γ. Moreover, Fig. 10 shows the isotherms with γ at Ri $=$ 10. The straight isotherms in the lower half of cavity at $\gamma = 0$, indicate the conduction heat transfer in this region.

Figs. 11–13 show U, θ along the cavity vertical centreline, and V along the horizontal centreline at Ri $=$ 0.1, Ri $=$ 1 and Ri $=$ 10 at $\varphi = 0.04$ for different γ's. Comparing these figures with Figs. 4–6 implies that an increase in φ would affect the flow properties more at Ri $=$ 10 than the state of Ri $=$ 0.1. More Ri corresponds to have more buoyancy motions especially

at larger γ; as well as Fig. 13 which shows U_{max} is larger than the moving lid velocity around $Y = 0.1$ and $Y = 0.9$ at $\gamma = 90$. This manner is due to combination of both buoyancy forces and lid motion effects and this phenomenon was not seen in Fig. 6 nor had it been seen in previous papers.

5.3. Effects of nanoparticles volume fraction

Fig. 14 concerns the nanofluid averaged Nusselt number (Nu_m) with a different φ and Ri at Re = 100. This figure shows the smallest amount of Nu_m is achieved at $\gamma = 0$; then it would approach to higher values with γ. However Nu_m mildly increases with γ at Ri = 0.1, its increasing rate is more significant at higher Ri (Ri = 1 and Ri = 10, respectively). More φ corresponds to large Nu_m so that using 4% of Cu nanoparticles leads to increase almost 50% of Nu_m at Ri = 0.1 for all values of γ. However, the variation of φ changes Nu_m in different ways at Ri = 10 from $\gamma = 0$ to $\gamma = 90$. Using 4% of Cu increases Nu_m slightly at Ri = 10 for $\gamma = 0$, but it severely increases for $\gamma = 90$. Fig. 14 implies the importance of using nanofluid to increase the heat transfer rate in the shallow inclined cavity. Larger values of γ and φ work well for this purpose especially at higher Ri.

So far, all results concerned fixed value of Reynolds number as Re = 100. To show the effect of Re on heat transfer rate, Nu_m with a different φ and Ri at Re = 10 is also studied. Its data is not shown here because of having brevity; however the appropriate performance of nanofluid to increase Nu_m with φ is well observed. In addition, the effect of γ at Ri = 0.1 and Ri = 1 is negligible. As a result, less value of Re corresponds to less effect of γ on Nu_m except at free convection domination. Moreover, larger amounts of Nu_m are achieved at Re = 100 than the state of Re = 10, for all cases.

6. Conclusion

Laminar mixed convection of water–Cu nanofluid in an inclined shallow lid driven cavity was studied by using lattice Boltzmann method for the first time. Boltzmann collision term and equations used to estimate the macroscopic properties and hydrodynamic boundary conditions were modified to include both buoyancy force and inclination angle. Present work showed the appropriate ability of LBM to simulate mixed convection of nanofluid in an inclined driven cavity.

The movement of cavity lid at Ri = 0.1 (force convection domination) has more effects on nanofluid than the state of Ri = 1 (mixed convection) and Ri = 10 (free convection). In the recent state, the buoyancy forces dominate the whole cavity space, and more sensitivity to γ is observed. Moreover, the combination effect of both buoyancy force and lid motion is able to drive the nanofluid faster than the upper wall velocity at $\gamma = 90$.

More φ corresponds to larger Nu_m; so that using 4% of Cu nanoparticles leads to increase almost 50% of Nu_m at force convection domination for all values of γ and Re = 100. Larger φ increases Nu_m slightly at free convection state for horizontal cavity but it severely increases Nu_m for the vertical position ($\gamma = 90$). More Nu_m is observed at Re = 100 than the state of Re = 10, which means most heat transfer rate can be achieved at vertical position of cavity at free convection domination for higher values of Re and volume fraction.

Acknowledgements

The third and last authors gratefully acknowledge the High Impact Research Grant UM.C/HIR/MOHE/ENG/45, UMRG Grant RP012D-13AET and University of Malaya, Malaysia, for the support in conducting this research work.

References

[1] S. Kandlikar, S. Garimella, D. Li, S. Colin, M.R. King, Heat transfer and fluid flow in minichannels and microchannels, 2006.
[2] X.D. Niu, C. Shu, Y.T. Chew, A thermal lattice Boltzmann model with diffuse scattering boundary condition for micro thermal flows, Comput. & Fluids 36 (2007) 273–281.
[3] J.A. Esfahani, A. Norouzi, Two relaxation time lattice Boltzmann model for rarefied gas flows, Physica A 393 (2014) 51–61.
[4] M. Gad-el-Hak, Flow physics in MEMS, Rev. Mec. Ind. 2 (2001) 313–341.
[5] X. Nie, G.D. Doolen, S. Chen, Lattice-Boltzmann simulation of fluid flows in MEMS, J. Stat. Phys. 107 (2002) 279–289.
[6] S. Chen, G.D. Doolen, Lattice Boltzmann method for fluid flows, Annu. Rev. Fluid Mech. 30 (1998) 329–364.
[7] Y. Zhou, R. Zhang, I. Staroselsky, H. Chen, W.T. Kim, M.S. Jhon, Simulation of micro- and nano-scale flows via the lattice Boltzmann method, Physica A 362 (2006) 68–77.
[8] A. Karimipour, A.H. Nezhad, A. D'Orazio, E. Shirani, Investigation of the gravity effects on the mixed convection heat transfer in a microchannel using lattice Boltzmann method, Int. J. Therm. Sci. 54 (2012) 142–152.
[9] G. Bird, Molecular Gas Dynamics and the Direct Simulation of Gas Flows, Oxford University Press, 1994.
[10] E.S. Oran, C.K. Oh, B.Z. Cybyk, Direct simulation Mont Carlo: recent advances and applications, Annu. Rev. Fluid Mech. 30 (1998) 403–441.
[11] H. Chen, S. Chen, W.M. Mathaaeus, Recovery of the Navier–Stokes equations using a lattice-gas Boltzmann method, Phys. Rev. A 45 (1992) 5339–5342.
[12] A. Tallavajhula, I. Kharagpur, U. Ruede, D. Bartuschat, Introduction to the Lattice Boltzmann Method, 10th Indo-German Winter Academy, 2011.
[13] P.L. Bhatnagar, E.P. Gross, M. Krook, A model for collision process in gases. I. Small amplitude processes in charged and neutral one-component system, Phys. Rev. 94 (1954) 511–522.
[14] S. Succi, The Lattice Boltzmann Equation for Fluid Dynamics and Beyond, Oxford University Press, Oxford, 2001.
[15] S. Chen, Lattice Boltzmann method for slip flow heat transfer in circular microtubes: extended Graetz problem, Appl. Math. Comput. 217 (2010) 3314–3320.
[16] S. Chen, Z. Tian, Entropy generation analysis of thermal micro-Couette flows in slip regime, Int. J. Therm. Sci. 49 (2010) 2211–2221.
[17] C.Y. Lim, C. Shu, X.D. Niu, Y.T. Chew, Application of lattice Boltzmann method to simulate microchannel flows, Phys. Fluids 14 (2002) 2299–2308.
[18] C. Shu, X.D. Niu, Y.T. Chew, A lattice Boltzmann kinetic model for microflow and heat transfer, J. Stat. Phys. 121 (2005) 239–255.

[19] V. Sofonea, R.F. Sekerka, Boundary conditions for the upwind finite difference lattice Boltzmann model: evidence of slip velocity in micro-channel flow, J. Comput. Phys. 207 (2005) 639–659.
[20] Y.H. Zhang, R.S. Qin, Y.H. Sun, R.W. Barber, D.R. Emerson, Gas flow in microchannels—a lattice Boltzmann method approach, J. Stat. Phys. 121 (2005) 257–267.
[21] W.C. Hung, Y. Ru, A numerical study for slip flow heat transfer, Appl. Math. Comput. 173 (2006) 1246–1264.
[22] Y. Xuan, Q. Li, M. Ye, Investigations of convective heat transfer in ferrofluid microflows using lattice-Boltzmann approach, Int. J. Therm. Sci. 46 (2007) 105–111.
[23] Z.W. Tian, C. Zou, H.J. Liu, Z.L. Guo, Z.H. Liu, C.G. Zheng, Lattice Boltzmann scheme for simulating thermal micro-flow, Physica A 385 (2007) 59–68.
[24] H. Babovsky, A numerical model for the Boltzmann equation with applications to micro flows, Comput. Math. Appl. 58 (2009) 791–804.
[25] S. Chen, Z. Tian, Simulation of microchannel flow using the lattice Boltzmann method, Physica A 388 (2009) 4803–4810.
[26] H.F. Oztop, I. Dagtekin, Mixed convection in two-sided lid-driven differentially heated square cavity, Int. J. Heat Mass Transfer 47 (2004) 1761–1769.
[27] A. Karimipour, M. Afrand, M. Akbari, M.R. Safaei, Simulation of Fluid Flow and Heat Transfer in the Inclined Enclosure, vol. 61, World Academy of Science, Engineering and Technology, 2012, pp. 435–440.
[28] M.R. Safaei, H.R. Goshayeshi, B.S. Razavi, M. Goodarzi, Numerical investigation of laminar and turbulent mixed convection in a shallow water-filled enclosure by various turbulence methods, Sci. Res. Essays 6 (22) (2011) 4826–4838.
[29] R. Iwatsu, J.M. Hyun, K. Kuwahara, Mixed convection in a driven cavity with a stable vertical temperature gradient, Int. J. Heat Mass Transfer 36 (1993) 1601–1608.
[30] A. D'Orazio, M. Corcione, G.P. Celata, Application to natural convection enclosed flows of a lattice Boltzmann BGK model coupled with a general purpose thermal boundary condition, Int. J. Therm. Sci. 43 (2004) 575–586.
[31] Y. Peng, C. Shu, Y.T. Chew, Simplified thermal lattice Boltzmann model for incompressible thermal flows, Phys. Rev. E 68 (2003) 026701-1-8.
[32] M. Jami, A. Mezrhab, M. Bouzidi, P. Lallemand, Lattice-Boltzmann computation of natural convection in a partitioned enclosure with inclined partitions attached to its hot wall, Physica A 368 (2007) 481–494.
[33] A. Grucelski, J. Pozorski, Lattice Boltzmann simulation of fluid flow in porous media of temperature-affected geometry, J. Theoret. Appl. Mech. 50 (2012) 193–214.
[34] X. He, S. Chen, G.D. Doolen, A novel thermal model for the lattice Boltzmann method in incompressible limit, J. Comput. Phys. 146 (1998) 282–300.
[35] A. Karimipour, A.H. Nezhad, A. D'Orazio, E. Shirani, The effects of inclination angle and Prandtl number on the mixed convection in the inclined lid driven cavity using lattice Boltzmann method, J. Theoret. Appl. Mech. 51 (2013) 447–462.
[36] S.U.S. Choi, Enhancing thermal conductivity of fluid with nanoparticles, in: Developments and Applications of Non-Newtonian Flow, ASME, 1995, pp. 99–105. FED 231/MD 66.
[37] H.F. Oztop, E. Abu-Nada, Numerical study of natural convection in partially heated rectangular enclosures filled with nanofluids, Int. J. Heat Fluid Flow 29 (2008) 1326–1336.
[38] R.K. Tiwari, M.K. Das, Heat transfer augmentation in a two-sided lid-driven differentially heated square cavity utilizing nanofluids, Int. J. Heat Mass Transfer 50 (2007) 2002–2018.
[39] R. Dehnavi, A. Rezvani, Numerical investigation of natural convection heat transfer of nanofluids in a C shaped cavity, Superlattices Microstruct. 52 (2012) 312–325.
[40] A.A. Arani, S.M. Sebdani, M. Mahmoodi, A. Ardeshiri, M. Aliakbari, Numerical study of mixed convection flow in a lid-driven cavity with sinusoidal heating on sidewalls using nanofluid, Superlattices Microstruct. 51 (2012) 893–911.
[41] M. Mahmoodi, S.M. Hashemi, Numerical study of natural convection of a nanofluid in C-shaped enclosures, Int. J. Therm. Sci. 55 (2012) 76–89.
[42] H.F. Oztop, M. Mobedi, E. Abu-Nada, I. Pop, A heatline analysis of natural convection in a square inclined enclosure filled with a CuO nanofluid under non-uniform wall heating condition, Int. J. Heat Mass Transfer 55 (2012) 5076–5086.
[43] O. Abouali, G. Ahmadi, Computer simulations of natural convection of single phase nanofluids in simple enclosures: a critical review, Appl. Therm. Eng. 36 (2012) 1–13.
[44] I. Pishkar, B. Ghasemi, Cooling enhancement of two fins in a horizontal channel by nanofluid mixed convection, Int. J. Therm. Sci. 59 (2012) 141–151.
[45] A. Karimipour, A.H. Nezhad, A. Behzadmehr, S. Alikhani, E. Abedini, Periodic mixed convection of a nanofluid in a cavity with top lid sinusoidal motion, Proc. IMechE Part C: J. Mech. Eng. Sci. 225 (2011) 2149–2160.
[46] M. Goodarzi, M.R. Safaei, K. Vafai, G. Ahmadi, M. Dahari, S.N. Kazi, N. Jomhari, Investigation of nanofluid mixed convection in a shallow cavity using a two-phase mixture model, Int. J. Therm. Sci. 75 (2014) 204–220.
[47] S. Mirmasoumi, A. Behzadmehr, Numerical study of laminar mixed convection of a nanofluid in a horizontal tube using two-phase mixture model, Appl. Therm. Eng. 28 (2008) 717–727.
[48] A.K. Santra, S. Sen, N. Chakraborty, Study of heat transfer due to laminar flow of copper–water nanofluid through two isothermally heated parallel plates, Int. J. Therm. Sci. 48 (2009) 391–400.
[49] M. Hassan, R. Sadri, G. Ahmadi, M.B. Dahari, S.N. Kazi, M.R. Safaei, E. Sadeghinezhad, Numerical study of entropy generation in a flowing nanofluid used in micro- and minichannels, Entropy 15 (2013) 144–155.
[50] G. Roy, I. Gherasim, F. Nadeau, G. Poitras, C.T. Nguyen, Heat transfer performance and hydrodynamic behavior of turbulent nanofluid radial flows, Int. J. Therm. Sci. 58 (2012) 120–129.
[51] S.M. Aminossadati, A. Raisi, B. Ghasemi, Effects of magnetic field on nanofluid forced convection in a partially heated microchannel, Int. J. Non-Linear Mech. 46 (2011) 1373–1382.
[52] Y. Guo, D. Qin, S. Shen, R. Bennacer, Nanofluid multi-phase convective heat transfer in closed domain: simulation with lattice Boltzmann method, Int. Commun. Heat Mass Transfer 39 (2012) 350–354.
[53] G.H.R. Kefayati, S.F. Hosseinizadeh, M. Gorji, H. Sajjadi, Lattice Boltzmann simulation of natural convection in tall enclosures using water/SiO_2 nanofluid, Int. Commun. Heat Mass Transfer 38 (2011) 798–805.
[54] F. Lai, Y. Yang, Lattice Boltzmann simulation of natural convection heat transfer of Al_2O_3/water nanofluids in a square enclosure, Int. J. Therm. Sci. 50 (2011) 1930–1941.
[55] E. Fattahi, M. Farhadi, K. Sedighi, H. Nemati, Lattice Boltzmann simulation of natural convection heat transfer in nanofluids, Int. J. Therm. Sci. 52 (2012) 137–144.
[56] M. Nabavitabatabayi, E. Shirani, M.H. Rahimian, Investigation of heat transfer enhancement in an enclosure filled with nanofluids using multiple relaxation time lattice Boltzmann modeling, Int. Commun. Heat Mass Transfer 38 (2011) 128–138.
[57] H. Nemati, M. Farhadi, K. Sedighi, E. Fattahi, A.A.R. Darzi, Lattice Boltzmann simulation of nanofluid in lid-driven cavity, Int. Commun. Heat Mass Transfer 37 (2010) 1528–1534.
[58] M.A.R. Sharif, Laminar mixed convection in shallow inclined driven cavities with hot moving lid on top and cooled from bottom, Appl. Therm. Eng. 27 (2007) 1036–1042.
[59] Y. Xuan, Q. Li, Investigation on convective heat transfer and flow features of nanofluids, ASME J. Heat Transfer 125 (2003) 151–155.
[60] H.C. Brinkman, The viscosity of concentrated suspensions and solutions, J. Chem. Phys. 20 (1952) 571–581.
[61] C.H. Chon, K.D. Kihm, S.P. Lee, S.U.S. Choi, Empirical correlation finding the role of temperature and particle size for nanofluid (Al_2O_3) thermal conductivity enhancement, Appl. Phys. Lett. 87 (2005) 153107–153107-3.
[62] S. Chapman, T.G. Cowling, The Mathematical Theory of Non-uniform Gases, third ed., Cambridge University Press, 1999.
[63] Y. Qian, D. Humie'res, P. Lallemand, Lattice BGK models for Navier–Stokes equation, Europhys. Lett. 17 (1992) 479–484.
[64] Q. Zou, X. He, On pressure and velocity boundary conditions for the lattice Boltzmann BGK model, Phys. Fluids 9 (1997) 1591–1598.